Submitted to the
International Conference on High Energy Physics
16-22 August 2004, Beijing, China

Abstract: 12-0255 **Session: BSM**

Search for lepton-flavor violation in *ep* collisions at HERA

ZEUS Collaboration

Abstract

A search for lepton-flavor violating interactions $e^{\pm}p \to \mu X$ and $e^{\pm}p \to \tau X$ has been performed with the ZEUS detector at HERA using an integrated luminosity of 130 pb^{-1}. The data were taken at the center-of-mass energy, $\sqrt{s}$, of 300 and 318 GeV. No evidence of lepton flavor violation was found and constraints were derived on Leptoquarks (LQs) that could mediate such interactions. For LQ masses below $\sqrt{s}$ limits were set on $\lambda_{eq_1}\sqrt{\beta_{\ell q}}$, where λ_{eq_1} is the coupling of the LQ to an electron and a first generation quark q_1 and $\beta_{\ell q}$ is the branching ratio of the LQ to the final state lepton ℓ (μ or τ) and a quark q. For LQ masses exceeding $\sqrt{s}$, limits were set on the four-fermion interaction term $\lambda_{eq_\alpha}\lambda_{\ell q_\beta}/M_{LQ}^2$ for LQs that couple to an electron and a quark q_α and to a lepton ℓ and a quark q_β. Some of the limits are also applicable to lepton-flavor violating processes mediated by squarks in R-parity-violating supersymmetric models. In some cases, expecially when a higher generation quark is involved and for the process $e^{\pm}p \to \tau X$, the ZEUS limits are the most stringent to date.

1 Introduction

The recent observations of neutrino oscillations [1, 2] have shown that lepton-flavor violation (LFV) does occur in the neutrino sector. Although the LFV induced in the charged lepton sector due to the neutrino oscillations could not be detected at the existent colliders due to the low rate [3], there are many extensions of the Standard Model (SM) like grand unified theories (GUT) [4], supersymmetries (SUSY) [5], compositeness [6] and technicolor [7] that predict $e \to \mu$ or $e \to \tau$ transitions detectable in sensitive experiments. In this analysis no evidence for LFV has been seen. The Buchmüller-Rückl-Wyler (BRW) leptoquark (LQ) model [8] and supersymmetry with R–Parity violation are used to give quantitative limits on the search. A detailed description of the cross section approximations used in this paper is given in the published 1994–97 e^+p data analysis [9].
At the HERA ep collider lepton-flavor violating interactions could be observed in the reaction $ep \to \ell X$ where ℓ is a μ or τ. Such processes are almost background free and would be a clear signal of physics beyond the Standard Model. There are strong constraints on LFV in several processes from low energy measurements of rare lepton and meson decay, muon-electron conversion on nuclei, etc. [10]; nevertheless HERA has a better sensitivity, expecially in the $e-\tau$ transition and when a second or third generation quark is involved. This analysis is based on the entire HERA I statistical sample collected by ZEUS in the years 1994 – 2000, corresponding to an integrated luminosity of $130\,\mathrm{pb}^{-1}$. These results supersede previous results published by ZEUS [9, 11].

2 The experimental conditions

A detailed description of the ZEUS detector can be found elsewhere [12]. In this section a brief outline of the main components used in this analysis is given: the central tracking detector (CTD) [13], the uranium-scintillator calorimeter (CAL) [14] and the forward muon detector (FMUON) [12].
The CTD, which is immersed in a magnetic field of 1.43 T provided by a superconducting solenoid, consists of 72 cylindrical drift chamber layers, organized in 9 superlayers covering the polar-angle[1] region $15^\circ < \theta < 164^\circ$. The transverse-momentum resolution for full-length tracks is $\sigma(p_T)/p_T = 0.0058 p_T \oplus 0.0065 \oplus 0.0014/p_T$, with p_T in GeV.
The CTD was also used to reconstruct the interaction vertex with a typical resolution of 4mm (1mm) in the Z (X and Y) coordinate.

[1] The ZEUS coordinate system is a right-handed Cartesian system, with the Z axis pointing in the proton beam direction, referred to as the "forward direction", and the X axis pointing left towards the center of HERA. The coordinate origin is at the nominal interaction point.

The high-resolution uranium–scintillator calorimeter consists of three parts: the forward (FCAL), the barrel (BCAL) and the rear (RCAL) calorimeters. Each part is subdivided transversely into towers and longitudinally into one electromagnetic section (EMC) and either one (in RCAL) or two (in BCAL and FCAL) hadronic sections (HAC). The smallest subdivision of the calorimeter is called a cell. The CAL energy resolutions, as measured under test-beam conditions, are $\sigma(E)/E = 0.18/\sqrt{E}$ for electrons and $\sigma(E)/E = 0.35/\sqrt{E}$ for hadrons (E in GeV). The FMUON detector consist of layers of streamer tubes and drift chambers. The magnetic fields of 1.6 T produced by two iron toroids placed at 9 m from the interaction point and of the iron yoke (1.4 T) placed around the CAL allow for the muon momentum measurement. The use of FMUON permits to extend the CTD acceptance for the high-momentum muon tracks in the polar region $8° < \theta < 20°$.
The luminosity was measured using the process $ep \to e\gamma p$. The small-angle photons were measured by the luminosity detector [15], a lead-scintillator calorimeter placed in the HERA tunnel at $Z = -107$ m.

3 Data samples and Monte Carlo simulation

The data used in this analysis was collected in the years 1994-2000 by the ZEUS experiment at HERA. The total integrated luminosity was $112 \pm 2.2\,\text{pb}^{-1}$ with e^+p collisions at the center-of-mass energy of 300 and 318 GeV and $16.7 \pm 0.3\,\text{pb}^{-1}$ with e^-p collision at $\sqrt{s} = 318$ GeV.
The signals for this analysis were taken to be LFV processes mediated by scalar or vector LQs. These were simulated by the Monte Carlo generator LQGENEP [16], which is based on the BRW model. The simulation of the hadronization and particle decays was performed using PYTHIA [17].
Various Monte Carlo samples were used to study the Standard Model background: charged current (CC) and neutral current (NC) deep inelastic scattering (DIS) were simulated using DJANGOH [18] an interface to the program HERACLES 4.6.1 [19] and LEPTO 6.5.1 [20]; HERWIG [21] was used for photoproduction background simulation and lepton pair production was simulated with GRAPE [22].

4 Kinematic quantities

In this section the most relevant kinematic quantities used in this analysis are introduced. Given E_i the energy measured in the i^{th} calorimeter cell and θ_i and ϕ_i its angles in a

spherical coordinate system, the total four–momentum in the CAL is (E, P_x, P_y, P_z) defined as $(\sum_i E_i, \sum_i E_i \sin\theta_i \cos\phi_i, \sum_i E_i \sin\theta_i \sin\phi_i, \sum_i E_i \cos\theta_i)$. The missing transverse momentum $\not{P}_t$, is hence given by $\sqrt{P_X^2 + P_Y^2}$, while the transverse energy, E_t, is defined as $\sum_i E_i \sin\theta_i$.
Another relevant quantity used in this analysis is $E - P_Z$. In the initial state $E - P_Z = 2E_e$ where E_e is the electron beam energy. If only particles in the very forward direction are lost, as in NC DIS events, $E - P_Z \sim 55\,\mathrm{GeV}$ in the final state.

5 $e - \mu$ transition

The characteristic of these events is a muon with a high transverse momentum balanced by a jet in the transverse plane. An apparent missing transverse momentum as measured by the calorimeter is due to the escape of the penetrating muon.

5.1 Muon identification

The muon identification is based on two different methods. The first method, used to identify muons in the polar angle range $16^\circ < \theta < 164^\circ$, required:

- A CTD track pointing to the vertex with transverse momentum (P_t^{trk}) above $5\,\mathrm{GeV}$ matching a calorimeter deposit compatible with a minimum ionizing particle;
- $D_{trk} > 0.5$ and $D_{jet} > 1$ where D_{trk} (D_{jet}) is the distance in the $\eta - \phi$ plane between the track associated to the muon and the closest track (jet);
- Muons in the polar angle region $115^\circ < \theta < 130^\circ$ were excluded to eliminate the background from the small number of electrons which lose a large fraction of their energy in the dead material between BCAL and RCAL.

Very forward muons ($8^\circ < \theta < 20^\circ$) were identified using reconstructed tracks in the FMUON detector.

5.2 Preselection

The trigger used in this analysis was identical to the one used in CC DIS measurement described elsewhere [23]. It was based on a cut on $\not{P}_t$ with a lower threshold than the one used in the offline analysis and described below. After applying cuts to reject background due to non ep collision (cosmics and beamgas interactions), the following pre-selection requirements were imposed:

- a reconstructed vertex with a Z coordinate, Z_{VTX}, not more than 50 cm from the nominal interaction point;
- $\not{P}_t > 15\,\mathrm{GeV}$;
- no electron candidate with energy larger than 10 GeV;
- An isolated muon candidate in the $\not{P}_t$ direction ($\Delta\phi < 20^\circ$, where $\Delta\phi$ is the difference between the azimuthal angle of the muon and the $\not{P}_t$ ϕ-direction).

The third cut was used to suppress NC DIS background.
Figure 1 shows the comparisons between data and MC expectations after the preselection. The sample contains 20 data events, while 25.9 ± 1.1 were expected from SM Monte Carlo, mainly from QED di-muon processes ($ep \to \mu^+\mu^- X$).

5.3 Final selection

The final selection was designed to reduce the SM background to a very low level. In addition to the preselection cuts the following cuts were applied:

- $\not{P}_t > 20\,\mathrm{GeV}$;
- $\not{P}_t/\sqrt{E_t} > 3\sqrt{\mathrm{GeV}}$;
- $E - P_Z + \Delta_\mu > 45\,\mathrm{GeV}$,

where $\Delta_\mu = \not{P}_t(1-\cos\theta_\mu)/\sin\theta_\mu$, θ_μ being the polar angle of the muon, is the contribution to $E - P_Z$ carried by the muon assuming that the transverse momentum of the muon is $\not{P}_t$. The second cut is used to reject high E_t photoproduction events where the $\not{P}_t$ can arise from the finite energy resolution.
No event satisfied the final cuts while 0.86 ± 0.15 were expected from the simulation of the SM background.
For LFV events mediated by a resonant production of a leptoquark the selection efficiency varied with the LQ mass and it ranged from 39% to 54% for scalar and from 47% to 62% for vector LQs with masses between 140 and 300 GeV.
For leptoquarks with mass much greater than the center of mass energy the efficiencies were almost independent of the LQ mass but varied with the initial generation of the quarks involved. Sea quarks in fact have a softer x distribution with respect to valence quarks which results in a lower momentum of the lepton in the final state, leading to a lower signal efficiency when an higher generation quark is involved. Therefore the selection efficiencies for high mass LQ was in the range 20 – 45%.

6 $e - \tau$ transition

Lepton-flavor violating events leading to a final state tau, are characterized by a high momentum isolated τ balanced by a jet in the transverse plane. Since the τ decays close to the interaction vertex, only its decay products are visible in the detector. Due to the presence of at least one neutrino in all the τ decay channels, a high value of $\not{P}_t$ is expected. Therefore for all the channels the CC DIS trigger (as for the muon channel) and a common preselection, requiring $\not{P}_t > 15\,\mathrm{GeV}$ and a reconstructed vertex with $|Z_{vtx}| < 50\,\mathrm{cm}$, was used.

6.1 Leptonic τ decays

For taus decaying into muons ($\tau \to \mu\bar{\nu}_\mu\nu_\tau$) the same selection cuts of the $ep \to \mu X$ were applied since the event topology is very similar.
For the $\tau \to e\bar{\nu}_e\nu_\tau$ channel the following cuts were applied after the common preselection:

- $20 < E - P_Z < 52\,\mathrm{GeV}$;
- no energy deposit in RCAL above $7\,\mathrm{GeV}$;
- $\not{P}_t/\sqrt{E_t} > 2.5\sqrt{\mathrm{GeV}}$;
- an electron with energy larger than $20\,\mathrm{GeV}$ in the polar angle region $8^\circ < \theta < 125^\circ$ and in the $\not{P}_t$ direction ($\Delta\phi < 20^\circ$).

6.2 Hadronic τ decays

Since jets coming from hadronic τ decays suffer from a large background from QCD jets, a tau finder was employed to distinguish the tau jets from the quark- and gluon-induced jets.

6.2.1 Tau identification

A detailed description of the tau finder can be found elsewhere [24,25]. The jet definition was based on the longitudinally invariant k_T cluster algorithm [26]. The jet shape was characterized by six observables [25]: the first ($rmean$) and the second ($rrms$) moment of the radial extension of the jet energy deposition; the first ($lmean$) and the second ($lrms$) moment of the energy deposition in the direction along the jet axis; the number of subjets (N_{subj}) with a y_{cut} of $5 \cdot 10^{-4}$ [27, 28]; the mass (M_{jet}) of the jet calculated from the calorimeter cells associated to the jet. In order to separate the signal from the background, the six variables were combined in a discriminant D, given, from any point in the phase space $\vec{x}(-\log(rmean), -\log(rrms), -\log(1-lmean), -\log(lrms), \mathrm{N_{subj}}, \mathrm{M_{jet}})$, as:

$$\mathrm{D}(\vec{x}) = \frac{\rho_{sig}(\vec{x})}{\rho_{sig}(\vec{x}) + \rho_{bg}(\vec{x})},$$

where ρ_{sig} and ρ_{bg} are the density functions of the signal and the background, respectively. Lepton-flavor violating events with the final state τ decaying into hadrons and a neutrino, were used to simulate the signal. The background simulation was based on CC DIS events. The densities, sampled using MC simulations, were calculated using a method which is based on range searching (PDE-RS) [29]. For any given jet with phase space coordinates $\vec{x}$, the signal and the background densities are evaluated from the number of corresponding signal and background jets in a 6-dimensional box of fixed size, which is centered around $\vec{x}$. The tau signal tends to have a large discriminant value ($\mathrm{D} \to 1$) while the CC DIS background has a low discriminant value ($\mathrm{D} \to 0$).

6.2.2 Preselection

The following cuts were applied for the preselection of the hadronic tau decays channel:

- No electron with energy larger than 10 GeV;
- $E_t > 50$ GeV;
- $15 < E - P_Z < 60$ GeV;
- a τ jet candidate (described below).

The τ jet candidate, was required to have a transverse momentum greater than 15 GeV, to be within the CTD acceptance ($15^\circ < \theta < 164^\circ$) and to have between one and three tracks pointing to the calorimeter deposition associated with the jet. Events with jets in the region between FCAL and BCAL ($36^\circ < \theta < 42^\circ$) were removed. In order to reject electrons from NC events a cut of 0.95 was applied on the electromagnetic energy fraction of the jet ($fEMC$). In addition the jet was required to satisfy the condition $ltf + fEMC < 1.6$, where ltf (the leading track fraction) was defined as the ratio between the momentum of the most energetic track in the jet and the jet energy.
Figures 2 and 3 show the comparison, after the preselection, between data and MC for the jet variables, the discriminant and $\Delta\phi$ distribution. After the hadronic preselection 119 events were found in data, while 131 ± 4 were expected from SM processes (CC and NC DIS, di-lepton producion, photoproduction), mainly from CC DIS.

6.2.3 Final selection

For the final selection the following further cuts were applied:

- the τ jet candidate was required to be aligned in azimuth, ϕ, with the direction of the $\not{P}_t$ ($|\Delta\phi| < 20°$),
- D > 0.9.

In Figure 4 the $\Delta\phi$ distribution of the 8 events with D > 0.9 is shown compared to SM expectation (11.2 ± 1.5 events).
No candidate was found in data for any of the three channels, while $1.7{\pm}0.4$ were predicted by Standard Model simulation.
The selection efficiency for low mass scalar (vector) LQs was in the range of $22 - 29\%$ ($23 - 34\%$), while for high mass LQs it was $4 - 20\%$.

7 Results

Since no evidence of lepton-flavor violating interactions was found, limits at 95% C.L. were set on the processes $ep \to \mu X$ and $ep \to \tau X$ mediated by a leptoquark.
In the low mass case ($M_{\rm LQ} < \sqrt{s}$) limits on the cross section were converted, using the narrow width approximation, in limits on $\lambda_{eq_1}\sqrt{\beta_{\ell q}}$, where λ_{eq_1} is the coupling between the leptoquark, the electron and a first generation quark, while $\beta_{\ell q}$ is the branching ratio of the leptoquark in lepton ℓ and a quark (u, d, s, c, b). For high mass ($M_{\rm LQ} \gg \sqrt{s}$) leptoquarks the cross section limits were converted, using the contact-interaction approximation, into limits on $\lambda_{eq_\alpha}\lambda_{\ell q_\beta}/M^2_{\rm LQ}$. The cross-sections were evaluated taking into account the QED initial state radiation and NLO QCD corrections (only for low mass scalar leptoquarks).

7.1 Low mass leptoquark and squark limits

Upper limits on $\lambda_{eq_1}\sqrt{\beta_{\mu q}}$ ($\lambda_{eq_1}\sqrt{\beta_{\tau q}}$) are shown in Figs. 5 and 6 (Figs. 7 and 8) for $F = 0$ and $|F| = 2$, scalar (a) and vector (b) LQs assuming resonantly produced leptoquarks as described in the BRW model. Since for sufficiently large LQ masses the cross-section is dominated by electron valence-quark fusion, only e^+p (e^-p) data were used to determine $F = 0$ ($|F| = -2$) LQs production limits. For couplings with electromagnetic strength ($\lambda_{eq_1} = \lambda_{\ell q_\beta} = 0.3 \approx \sqrt{4\pi\alpha}$) LQ with masses up to 300 GeV can be excluded at 95% C.L. Alternatively for a fixed $M_{\rm LQ}$ of 250 GeV values of $\lambda_{eq_1}\sqrt{\beta_{\mu q}}$ ($\lambda_{eq_1}\sqrt{\beta_{\tau q}}$) down to 0.010 (0.012) can be excluded. Costraints on $\lambda_{eq_1}\sqrt{\beta_{\mu q}}$ ($\lambda_{eq_1}\sqrt{\beta_{\tau q}}$) for $\tilde{S}^L_{1/2}$ and for S^L_0 can be interpreted as limits on $\lambda'_{1j1}\sqrt{\beta_{\tilde{u}^j\to\ell q}}$ and $\lambda'_{11k}\sqrt{\beta_{\tilde{d}^k\to\ell q}}$ for $\tilde{u}^j$ and $\tilde{d}^k$ R parity violating squarks respectively [30]. In Tables 1, 2, 3 and 4 the limits for the μ- and τ-channels obtained fixing the mass or the coupling are reported for F=0 and F=2 LQs.

7.2 High mass leptoquarks and squarks limits ($M_{\rm LQ} \gg \sqrt{s}$)

Tables 9 and 9 show the 95% C.L. limits on $\lambda_{eq_\alpha}\lambda_{\mu q_\beta}/M_{\rm LQ}^2$ (third row of each cell) for $F=0$ and $|F|=2$ high mass leptoquarks coupling to eq_α and μq_β. Limits were evaluated for all combinations of quark generations α, β, excluding when a t-quark would be involved. Tables 9 and 9 show the corresponding limits for LQs coupling to eq_α and τq_β. Limits on $\lambda_{eq_\alpha}\lambda_{\mu q_\beta}/M_{\rm LQ}^2$ for $\tilde{S}^L_{1/2}$ and for S^L_0 LQs correspond to limits on $\lambda'_{1jk}\lambda'_{1jk'}/M^2_{\tilde{u}}$ for a u-type squark of generation j and on $\lambda'_{1jk}\lambda'_{1j'k}/M^2_{\tilde{d}}$ for a d-type squark of generation k respectively.

8 Comparison with limits from other experiments

8.1 Low energy experiments

There are many constraints from low energy experiments on lepton flavor violating processes coming mainly from rare lepton or mesons decays. Most of them can be converted into limits on massive scalar or vector leptoquark exchange [10]. In Tables 9-9 the limits coming from such measurements are compared to the constraints coming from this analysis. For the $e-\mu$ transition indirect limits are very tight and ZEUS limits are better only in the few cases when the c-quark is involved. In the $e-\tau$ case ZEUS improves the existing limits for many initial and final state quark combinations expecially when a quark of the second or third generation is involved. Assuming $\lambda_{eq_1} = \lambda_{\ell q_\beta}$ ZEUS limits on low mass LQs can be compared to the limits from low energy experiments. In Figs. 5 and 6(c-d) limits on λ_{eq_1} as function of the LQ mass are compared to the limits coming from $e-\mu$ conversion in nuclei and from rare K and B meson decays. ZEUS limits are better or competitive with indirect limits up to $\sim 250\,\mathrm{GeV}$ when the quark in the final state is of the third generation. In Figs. 7 and 8(c-d) the corresponding limits for the τ case are shown compared to constraints coming from rare τ, B or K decays. In this case ZEUS limits are competitive in most of the cases in almost all the mass range accessible with HERA.

8.2 LFV at colliders

Tevatron limits are complementary to the ZEUS ones since they do not depend on the Yukawa coupling. Moreover LQs are assumed to couple only with one lepton generation; therefore they do not induce necessarily lepton-flavor violating interactions. The CDF and DØ collaboration exclude scalar LQs coupling exclusively to μq with mass up to 202 GeV [31] and 200 GeV [32] respectively. CDF performed an analysis searching for leptoquarks which couple exclusively to the third generation of leptons and excluded LQs with $M_{\mathrm{LQ}} < 99\,\mathrm{GeV}$ if $\beta_{\tau b} = 1$. The DØ collaboration looking for $\nu\nu bb$ final states excluded LQs with masses below 94 GeV if $\beta_{\nu b} = 1$.
H1 performed an analysis on lepton-flavor violation [33] similar to the present one using $37\,\mathrm{pb}^{-1}$ of data at the center of mass energy of 300 GeV.

9 Conclusions

The data taken by the ZEUS experiment at HERA in e^+p and e^-p interactions at the center of mass energy of 300 GeV and 318 GeV during the years 1994-2000 corresponding to an integrated luminosity of $130\,\mathrm{pb}^{-1}$ were analysed searching for LFV. Both μ and τ channel were analysed. No evidence of lepton-flavor violating interactions was found. Limits at 95% C.L. were set on $\lambda_{eq_i}\sqrt{\beta_{\ell q_\beta}}$ as a function of the mass for LQ bosons with mass lower than the center of mass energy. For electromagnetic coupling constant ($\lambda_{eq_1} = \lambda_{\ell q_\beta} = 0.3$) mass limits between 265 and 300 GeV were set on the different LQ types. For $M_{\mathrm{LQ}} = 250\,\mathrm{GeV}$ upper limits on $\lambda_{eq_i}\sqrt{\beta_{\mu q_\beta}}$ ($\lambda_{eq_i}\sqrt{\beta_{\tau q_\beta}}$) in the range $0.010 - 0.11$ ($0.012 - 0.13$) were set.
For LQs with $M_{\mathrm{LQ}} \gg \sqrt{s}$ upper limits on $\lambda_{eq_\alpha}\lambda_{\mu q_\beta}/M_{\mathrm{LQ}}$ and $\lambda_{eq_\alpha}\lambda_{\tau q_\beta}/M_{\mathrm{LQ}}$ were calculated for all combinations of initial and final state quark generations.
Some of the limits also apply to R-Parity violating squarks. In many cases, expecially in the τ-channel, ZEUS limits are more stringent than any other limit published to date.

References

[1] Super-Kamiokande Coll., Y. Fukuda et al., Phys. Rev. Lett. **81**, 1562 (1998).

[2] SNO Coll., Q.R. Ahmad et al., Phys. Rev. Lett. **87**, 071301 (2001).

[3] Illana, Jose I. and Masip, Manuel, Acta Phys. Polon. **B34**, 5413 (2003).

[4] J.C. Pati and A. Salam, Phys. Rev. **D 10**, 275 (1974);
H. Georgi and S.L. Glashow, Phys. Rev. Lett. **32**, 438 (1974);
P. Langacker, Phys. Rep. **72**, 185 (1981).

[5] H.P. Nilles, Phys. Rep. **110**, 1 (1984);
H.E. Haber and G.L. Kane, Phys. Rep. **117**, 75 (1985).

[6] B. Schrempp and F. Schrempp, Phys. Lett. **B 153**, 101 (1985);
J. Wudka, Phys. Lett. **B 167**, 337 (1986).

[7] S. Dimopoulos and L. Susskind, Nucl. Phys. **B 155**, 237 (1979);
S. Dimopoulos, Nucl. Phys. **B 168**, 69 (1980);
E. Farhi and L. Susskind, Phys. Rev. **D 20**, 3404 (1979);
E. Farhi and L. Susskind, Phys. Rep. **74**, 277 (1981).

[8] W. Buchmüller, R. Rückl and D. Wyler, Phys. Lett. **B 191**, 442 (1987). Erratum in Phys. Lett. **B 448**, 320 (1999).

[9] ZEUS Coll., S. Chekanov et al., Phys. Rev. **D 65**, 92004 (2002).

[10] S. Davidson, D. Bailey and B.A. Campbell, Z. Phys. **C 61**, 613 (1994);
E. Gabrielli, Phys. Rev. **D 62**, 055009 (2000);
Herz, Margarete, *Bounds on leptoquark and supersymmetric, R-parity violating interactions from meson decays. (In German).* Thesis, Report hep-ph/0301079, 2002.

[11] ZEUS Coll., M. Derrick et al., Z. Phys. **C 73**, 613 (1997).

[12] ZEUS Coll., U. Holm (ed.), *The ZEUS Detector*. Status Report (unpublished), DESY (1993), available on `http://www-zeus.desy.de/bluebook/bluebook.html`.

[13] N. Harnew et al., Nucl. Inst. Meth. **A 279**, 290 (1989);
B. Foster et al., Nucl. Phys. Proc. Suppl. **B 32**, 181 (1993);
B. Foster et al., Nucl. Inst. Meth. **A 338**, 254 (1994).

[14] M. Derrick et al., Nucl. Inst. Meth. **A 309**, 77 (1991);
A. Andresen et al., Nucl. Inst. Meth. **A 309**, 101 (1991);
A. Caldwell et al., Nucl. Inst. Meth. **A 321**, 356 (1992);
A. Bernstein et al., Nucl. Inst. Meth. **A 336**, 23 (1993).

[15] J. Andruszków et al., Preprint DESY-92-066, DESY, 1992;
ZEUS Coll., M. Derrick et al., Z. Phys. **C 63**, 391 (1994);
J. Andruszków et al., Acta Phys. Pol. **B 32**, 2025 (2001).

[16] L. Bellagamba, Comp. Phys. Comm. **141**, 83 (2001).

[17] T. Sjöstrand, Comp. Phys. Comm. **82**, 74 (1994).

[18] H. Spiesberger, HERACLES *and* DJANGOH*: Event Generation for ep Interactions at HERA Including Radiative Processes*, 1998, available on
`http://www.desy.de/~hspiesb/djangoh.html`.

[19] A. Kwiatkowski, H. Spiesberger and H.-J. Möhring, Comp. Phys. Comm. **69**, 155 (1992). Also in *Proc. Workshop Physics at HERA*, 1991, DESY, Hamburg;
H. Spiesberger, *An Event Generator for ep Interactions at HERA Including Radiative Processes (Version 4.6)*, 1996, available on
`http://www.desy.de/~hspiesb/heracles.html`.

[20] G. Ingelman, A. Edin and J. Rathsman, Comp. Phys. Comm. **101**, 108 (1997).

[21] G. Marchesini et al., Comp. Phys. Comm. **67**, 465 (1992).

[22] T. Abe, Comp. Phys. Comm. **136**, 126 (2001).

[23] ZEUS Coll., J. Breitweg et al., Eur. Phys. J. **C 12**, 411 (2000).

[24] C.N. Nguyen. Diploma Thesis, Universität Hamburg, Hamburg, Germany, Report DESY-THESIS-2002-024, 2002.

[25] Chekanov, S. and others, Phys. Lett. **B583**, 41 (2004).

[26] S.Catani et al., Nucl. Phys. **B406**, 187 (1993);
S.D. Ellis and D.E. Soper, Phys. Rev. **D 48**, 3160 (1993).

[27] Forshaw, J. R. and Seymour, M. H., JHEP **09**, 009 (1999).

[28] Seymour, Michael H., Nucl. Phys. **B421**, 545 (1994).

[29] T. Carli and B. Koblitz. Batavia, USA, 2000, Adv. Comp. Analysis Techniques in Phys. Research P. Bath and M. Kasemann, Eds., pp 110, also in hep-ph/0011224, 2000;
T. Carli and B. Koblitz, Nucl. Inst. Meth. **A501**, 576 (2003).

[30] J. Butterworth and H. Dreiner, Nucl. Phys. **B 397**, 3 (1993).

[31] CDF Coll., F. Abe et al., Phys. Rev. Lett. **81**, 4806 (1998).

[32] DØ Coll., B. Abbott et al., Phys. Rev. Lett. **84**, 2088 (2000).

[33] H1 Coll., C. Adloff et al., Eur. Phys. J. **C 11**, 447 (1999). Erratum in
Eur. Phys. J. C14, 553 (2000).

LQ type	$\tilde{S}^L_{1/2}$	$S^L_{1/2}$	$S^R_{1/2}$	V^L_0	V^R_0	$\tilde{V}^R_0$	V^L_1
μ-channel limit on $M_{\mathrm{LQ}}[\,\mathrm{GeV}]$	278	294	294	279	283	297	300
τ-channel limit on $M_{\mathrm{LQ}}[\,\mathrm{GeV}]$	275	292	292	276	281	295	299

Table 1: 95% *C.L. lower limits on* M_{LQ} *for* $F = 0$ *LQs in the* μ*- and the* τ*-channels assuming* $\lambda_{eq_1} = \lambda_{\ell q} = 0.3$.

LQ type	S^L_0	S^R_0	$\tilde{S}^R_0$	S^L_1	$V^L_{1/2}$	$V^R_{1/2}$	$\tilde{V}^R_{1/2}$
μ-channel limit on $M_{\mathrm{LQ}}[\,\mathrm{GeV}]$	279	285	265	282	273	290	289
τ-channel limit on $M_{\mathrm{LQ}}[\,\mathrm{GeV}]$	275	282	261	279	269	287	287

Table 2: 95% *C.L. lower limits on* M_{LQ} *for* $|F| = 2$ *LQs in the* μ*- and the* τ*-channels assuming* $\lambda_{eq_1} = \lambda_{\ell q} = 0.3$.

LQ type	$\tilde{S}^L_{1/2}$	$S^L_{1/2}$	$S^R_{1/2}$	V^L_0/V^R_0	$\tilde{V}^R_0$	V^L_1
μ-channel limit on $\lambda_{eq_1}\sqrt{\beta_{\mu q}}$	0.050	0.021	0.019	0.034	0.015	0.010
τ-channel limit on $\lambda_{eq_1}\sqrt{\beta_{\tau q}}$	0.061	0.025	0.023	0.042	0.018	0.012

Table 3: 95% *C.L. upper limits on* $\lambda_{eq_1}\sqrt{\beta_{\ell q}}$ *for* $F = 0$ *LQs with mass* $M_{\mathrm{LQ}} = 250$ *GeV in the* μ*- and the* τ*-channels.*

LQ type	S^L_0/S^R_0	$\tilde{S}^R_0$	S^L_1	$V^L_{1/2}$	$V^R_{1/2}$	$\tilde{V}^R_{1/2}$
μ-channel limit on $\lambda_{eq_1}\sqrt{\beta_{\mu q}}$	0.047	0.109	0.040	0.074	0.030	0.033
τ-channel limit on $\lambda_{eq_1}\sqrt{\beta_{\tau q}}$	0.057	0.133	0.049	0.093	0.038	0.041

Table 4: 95% *C.L. upper limits on* $\lambda_{eq_1}\sqrt{\beta_{\ell q}}$ *for* $|F| = 2$ *LQs with mass* $M_{\mathrm{LQ}} = 250$ *GeV in the* μ*- and the* τ*-channels.*

$e \to \mu$			ZEUS (prel.) $e^{\pm}p$ 94-00				$F=0$
$\alpha\beta$	$S^L_{1/2}$ $e^-\bar{u}$ e^+u	$S^R_{1/2}$ $e^-(\bar{u}+\bar{d})$ $e^+(u+d)$	$\tilde{S}^L_{1/2}$ $e^-\bar{d}$ e^+d	V^L_0 $e^-\bar{d}$ e^+d	V^R_0 $e^-\bar{d}$ e^+d	$\tilde{V}^R_0$ $e^-\bar{u}$ e^+u	V^L_1 $e^-(\sqrt{2}\bar{u}+\bar{d})$ $e^+(\sqrt{2}u+d)$
1 1	$\mu N \to eN$ 5.2×10^{-5} **1.1**	$\mu N \to eN$ 2.6×10^{-5} **0.9**	$\mu N \to eN$ 5.2×10^{-5} **1.6**	$\mu N \to eN$ 2.6×10^{-5} **1.0**	$\mu N \to eN$ 2.6×10^{-5} **1.0**	$\mu N \to eN$ 2.6×10^{-5} **0.8**	$\mu N \to eN$ 0.8×10^{-5} **0.4**
1 2	$D \to \mu\bar{e}$ 2.4 $\boxed{\mathbf{1.2}}$	$K \to \mu\bar{e}$ 2×10^{-5} **1.0**	$K \to \mu\bar{e}$ 2×10^{-5} **1.7**	$K \to \mu\bar{e}$ 1×10^{-5} **1.2**	$K \to \mu\bar{e}$ 1×10^{-5} **1.2**	$D \to \mu\bar{e}$ 1.2 $\boxed{\mathbf{1.0}}$	$K \to \mu\bar{e}$ 1×10^{-5} **0.4**
1 3	*	$B \to \mu\bar{e}$ 0.4 **1.7**	$B \to \mu\bar{e}$ 0.4 **1.8**	$B \to \mu\bar{e}$ 0.2 **1.5**	$B \to \mu\bar{e}$ 0.2 **1.5**	*	$B \to \mu\bar{e}$ 0.2 **1.5**
2 1	$D \to \mu\bar{e}$ 2.4 **3.6**	$K \to \mu\bar{e}$ 2×10^{-5} **2.4**	$K \to \mu\bar{e}$ 2×10^{-5} **3.1**	$K \to \mu\bar{e}$ 1×10^{-5} **1.3**	$K \to \mu\bar{e}$ 1×10^{-5} **1.3**	$D \to \mu\bar{e}$ 1.2 **1.2**	$K \to \mu\bar{e}$ 1×10^{-5} **0.6**
2 2	$\mu N \to eN$ 9.2×10^{-4} **5.6**	$\mu N \to eN$ 1.3×10^{-3} **3.1**	$\mu N \to eN$ 3×10^{-3} **3.7**	$\mu N \to eN$ 1.5×10^{-3} **1.9**	$\mu N \to eN$ 1.5×10^{-3} **1.9**	$\mu N \to eN$ 4.6×10^{-4} **2.8**	$\mu N \to eN$ 2.7×10^{-4} **1.1**
2 3	*	$B \to \bar{\mu}eK$ 0.3 **4.2**	$B \to \bar{\mu}eK$ 0.3 **4.1**	$B \to \bar{\mu}eK$ 0.15 **2.9**	$B \to \bar{\mu}eK$ 0.15 **2.9**	*	$B \to \bar{\mu}eK$ 0.15 **2.9**
3 1	*	$B \to \mu\bar{e}$ 0.4 **4.4**	$B \to \mu\bar{e}$ 0.4 **4.4**	V_{ub} 0.12 **1.5**	$B \to \mu\bar{e}$ 0.2 **1.5**	*	V_{ub} 0.12 **1.5**
3 2	*	$B \to \bar{\mu}eK$ 0.3 **5.8**	$B \to \bar{\mu}eK$ 0.3 **5.8**	$B \to \bar{\mu}eK$ 0.15 **2.2**	$B \to \bar{\mu}eK$ 0.15 **2.2**	*	$B \to \bar{\mu}eK$ 0.15 **2.2**
3 3	*	$\mu N \to eN$ 1.3×10^{-3} **7.6**	$\mu N \to eN$ 3×10^{-3} **7.6**	$\mu N \to eN$ 1.5×10^{-3} **4.0**	$\mu N \to eN$ 1.5×10^{-3} **4.0**	*	$\mu N \to eN$ 2.7×10^{-4} **4.0**

$e \to \mu$			ZEUS (prel.) $e^{\pm}p$ 94-00			$\|F\| = 2$
$\alpha\beta$	S_0^L e^-u $e^+\bar{u}$	S_0^R e^-u $e^+\bar{u}$	$\tilde{S}_0^R$ e^-d $e^+\bar{d}$	S_1^L $e^-(u+\sqrt{2}d)$ $e^+(\bar{u}+\sqrt{2}\bar{d})$	$V_{1/2}^L$ e^-d $e^+\bar{d}$	$V_{1/2}^R$ $e^-(u+d)$ $e^+(\bar{u}+\bar{d})$	$\tilde{V}_{1/2}^L$ e^-u $e^+\bar{u}$
1 1	$\mu N \to eN$ 5.2×10^{-5} **1.6**	$\mu N \to eN$ 5.2×10^{-5} **1.6**	$\mu N \to eN$ 5.2×10^{-5} **2.0**	$\mu N \to eN$ 1.7×10^{-5} **0.9**	$\mu N \to eN$ 2.6×10^{-5} **0.8**	$\mu N \to eN$ 1.3×10^{-5} **0.5**	$\mu N \to eN$ 2.6×10^{-5} **0.6**
1 2	$K \to \pi\nu\bar{\nu}$ 10^{-3} **2.4**	$D \to \mu\bar{e}$ 2.4 **2.4**	$K \to \mu\bar{e}$ 2×10^{-5} **2.5**	$K \to \mu\bar{e}$ 1×10^{-5} **1.1**	$K \to \mu\bar{e}$ 1×10^{-5} **1.6**	$K \to \mu\bar{e}$ 1×10^{-5} **1.2**	$D \to \mu\bar{e}$ 1.2 **1.7**
1 3	*	*	$B \to \mu\bar{e}$ 0.4 **2.8**	V_{ub} 0.24 **1.4**	$B \to \mu\bar{e}$ 0.2 **2.2**	$B \to \mu\bar{e}$ 0.2 **2.2**	*
2 1	$K \to \pi\nu\bar{\nu}$ 10^{-3} **2.1**	$D \to \mu\bar{e}$ 2.4 $\boxed{\mathbf{2.1}}$	$K \to \mu\bar{e}$ 2×10^{-5} **2.5**	$K \to \mu\bar{e}$ 1×10^{-5} **1.1**	$K \to \mu\bar{e}$ 1×10^{-5} **0.9**	$K \to \mu\bar{e}$ 1×10^{-5} **0.5**	$D \to \mu\bar{e}$ 1.2 $\boxed{\mathbf{0.6}}$
2 2	$\mu N \to eN$ 9.2×10^{-4} **5.6**	$\mu N \to eN$ 9.2×10^{-4} **5.6**	$\mu N \to eN$ 3×10^{-3} **3.7**	$\mu N \to eN$ 2.5×10^{-3} **1.8**	$\mu N \to eN$ 1.5×10^{-3} **1.9**	$\mu N \to eN$ 6.7×10^{-4} **1.6**	$\mu N \to eN$ 4.6×10^{-4} **2.8**
2 3	*	*	$B \to \bar{\mu}eK$ 0.3 **4.3**	$B \to \bar{\mu}eK$ 0.15 **2.2**	$B \to \bar{\mu}eK$ 0.15 **2.9**	$B \to \bar{\mu}eK$ 0.15 **2.9**	*
3 1	*	*	$B \to \mu\bar{e}$ 0.4 **3.1**	$B \to \mu\bar{e}$ 0.4 **1.6**	$B \to \mu\bar{e}$ 0.2 **1.0**	$B \to \mu\bar{e}$ 0.2 **1.0**	*
3 2	*	*	$B \to \bar{\mu}eK$ 0.3 **5.9**	$B \to \bar{\mu}eK$ 0.15 **2.9**	$B \to \bar{\mu}eK$ 0.15 **2.2**	$B \to \bar{\mu}eK$ 0.15 **2.2**	*
3 3	*	*	$\mu N \to eN$ 3×10^{-3} **7.7**	$\mu N \to eN$ 2.5×10^{-3} **3.8**	$\mu N \to eN$ 1.5×10^{-3} **4.0**	$\mu N \to eN$ 6.7×10^{-4} **4.0**	*

$e \to \tau$ ZEUS (prel.) $e^{\pm}p$ 94-00 $F = 0$

$\alpha\beta$	$S^L_{1/2}$ $e^-\bar{u}$ e^+u	$S^R_{1/2}$ $e^-(\bar{u}+\bar{d})$ $e^+(u+d)$	$\tilde{S}^L_{1/2}$ $e^-\bar{d}$ e^+d	V^L_0 $e^-\bar{d}$ e^+d	V^R_0 $e^-\bar{d}$ e^+d	$\tilde{V}^R_0$ $e^-\bar{u}$ e^+u	V^L_1 $e^-(\sqrt{2}\bar{u}+\bar{d})$ $e^+(\sqrt{2}u+d)$
1 1	$\tau \to \pi e$ 0.4 **1.7**	$\tau \to \pi e$ 0.2 **1.4**	$\tau \to \pi e$ 0.4 **2.6**	$\tau \to \pi e$ 0.2 **1.7**	$\tau \to \pi e$ 0.2 **1.7**	$\tau \to \pi e$ 0.2 **1.2**	$\tau \to \pi e$ 0.06 **0.6**
1 2	$\boxed{\mathbf{1.8}}$	$\tau \to Ke$ 6.3 $\boxed{\mathbf{1.5}}$	$K \to \pi\nu\bar{\nu}$ 5.8×10^{-4} **2.8**	$\tau \to Ke$ 3.2 $\boxed{\mathbf{2.1}}$	$\tau \to Ke$ 3.2 $\boxed{\mathbf{2.1}}$	$\boxed{\mathbf{1.5}}$	$K \to \pi\nu\bar{\nu}$ 1.5×10^{-4} **0.7**
1 3	*	$B \to \tau\bar{e}$ 0.6 **3.0**	$B \to \tau\bar{e}$ 0.6 **3.1**	$B \to \tau\bar{e}$ 0.3 **2.5**	$B \to \tau\bar{e}$ 0.3 **2.5**	*	$B \to \tau\bar{e}$ 0.3 **2.5**
2 1	$\boxed{\mathbf{6.1}}$	$\tau \to Ke$ 6.3 $\boxed{\mathbf{4.1}}$	$K \to \pi\nu\bar{\nu}$ 5.8×10^{-4} **5.2**	$\tau \to Ke$ 3.2 $\boxed{\mathbf{2.3}}$	$\tau \to Ke$ 3.2 $\boxed{\mathbf{2.3}}$	$\boxed{\mathbf{2.2}}$	$K \to \pi\nu\bar{\nu}$ 1.5×10^{-4} **1.0**
2 2	$\tau \to 3e$ 5 **10**	$\tau \to 3e$ 8 $\boxed{\mathbf{5.5}}$	$\tau \to 3e$ 17 $\boxed{\mathbf{6.5}}$	$\tau \to 3e$ 9 $\boxed{\mathbf{3.4}}$	$\tau \to 3e$ 9 $\boxed{\mathbf{3.4}}$	$\tau \to 3e$ 3 **5.5**	$\tau \to 3e$ 1.6 **2.1**
2 3	*	$B \to \tau\bar{e}X$ 14 $\boxed{\mathbf{8.0}}$	$B \to \tau\bar{e}X$ 14 $\boxed{\mathbf{7.7}}$	$B \to \tau\bar{e}X$ 7.2 $\boxed{\mathbf{5.4}}$	$B \to \tau\bar{e}X$ 7.2 $\boxed{\mathbf{5.4}}$	*	$B \to \tau\bar{e}X$ 7.2 $\boxed{\mathbf{5.4}}$
3 1	*	$B \to \tau\bar{e}$ 0.6 **7.9**	$B \to \tau\bar{e}$ 0.6 **7.3**	V_{ub} 0.12 **2.6**	$B \to \tau\bar{e}$ 0.3 **2.6**	*	V_{ub} 0.12 **2.6**
3 2	*	$B \to \tau\bar{e}X$ 14 $\boxed{\mathbf{11}}$	$B \to \tau\bar{e}X$ 14 $\boxed{\mathbf{10}}$	$B \to \tau\bar{e}X$ 7.2 $\boxed{\mathbf{4.2}}$	$B \to \tau\bar{e}X$ 7.2 $\boxed{\mathbf{4.2}}$	*	$B \to \tau\bar{e}X$ 7.2 $\boxed{\mathbf{4.2}}$
3 3	*	$\tau \to 3e$ 8 **15**	$\tau \to 3e$ 17 $\boxed{\mathbf{14}}$	$\tau \to 3e$ 9 $\boxed{\mathbf{8.2}}$	$\tau \to 3e$ 9 $\boxed{\mathbf{8.2}}$	*	$\tau \to 3e$ 1.6 **8.2**

$e \to \tau$	ZEUS (prel.) $e^{\pm}p$ 94-00						$\lvert F \rvert = 2$
$\alpha\beta$	S_0^L e^-u $e^+\bar{u}$	S_0^R e^-u $e^+\bar{u}$	$\tilde{S}_0^R$ e^-d $e^+\bar{d}$	S_1^L $e^-(u+\sqrt{2}d)$ $e^+(\bar{u}+\sqrt{2}\bar{d})$	$V_{1/2}^L$ e^-d $e^+\bar{d}$	$V_{1/2}^R$ $e^-(u+d)$ $e^+(\bar{u}+\bar{d})$	$\tilde{V}_{1/2}^L$ e^-u $e^+\bar{u}$
1 1	G_F 0.3 **2.5**	$\tau \to \pi e$ 0.4 **2.5**	$\tau \to \pi e$ 0.4 **3.4**	$\tau \to \pi e$ 0.1 **1.4**	$\tau \to \pi e$ 0.2 **1.4**	$\tau \to \pi e$ 0.1 **0.8**	$\tau \to \pi e$ 0.2 **1.0**
1 2	$K \to \pi\nu\bar{\nu}$ 5.8×10^{-4} **3.8**	$\boxed{\mathbf{3.8}}$	$\tau \to Ke$ 6.3 $\boxed{\mathbf{4.3}}$	$K \to \pi\nu\bar{\nu}$ 2.9×10^{-4} **1.8**	$K \to \pi\nu\bar{\nu}$ 2.9×10^{-4} **2.8**	$\tau \to Ke$ 3.2 $\boxed{\mathbf{2.0}}$	$\boxed{\mathbf{3.0}}$
1 3		$*$	$B \to \tau\bar{e}$ 0.6 **5.0**	V_{ub} 0.12 **2.5**	$B \to \tau\bar{e}$ 0.3 **3.9**	$B \to \tau\bar{e}$ 0.3 **3.9**	$*$
2 1	$K \to \pi\nu\bar{\nu}$ 5.8×10^{-4} **3.3**	$\boxed{\mathbf{3.3}}$	$\tau \to Ke$ 6.3 $\boxed{\mathbf{4.3}}$	$K \to \pi\nu\bar{\nu}$ 2.9×10^{-4} **1.8**	$K \to \pi\nu\bar{\nu}$ 2.9×10^{-4} **1.5**	$\tau \to Ke$ 3.2 $\boxed{\mathbf{0.8}}$	$\boxed{\mathbf{1.0}}$
2 2	$\tau \to 3e$ 5 **10**	$\tau \to 3e$ 5 **10**	$\tau \to 3e$ 17 $\boxed{\mathbf{6.4}}$	$\tau \to 3e$ 14 $\boxed{\mathbf{3.2}}$	$\tau \to 3e$ 9 $\boxed{\mathbf{3.5}}$	$\tau \to 3e$ 4 $\boxed{\mathbf{2.8}}$	$\tau \to 3e$ 3 **5.1**
2 3	$*$	$*$	$B \to \tau\bar{e}X$ 14 $\boxed{\mathbf{8.2}}$	$B \to \tau\bar{e}X$ 7.2 $\boxed{\mathbf{4.1}}$	$B \to \tau\bar{e}X$ 7.2 $\boxed{\mathbf{5.3}}$	$B \to \tau\bar{e}X$ 7.2 $\boxed{\mathbf{5.3}}$	$*$
3 1	$*$	$*$	$B \to \tau\bar{e}$ 0.6 **5.4**	$B \to \tau\bar{e}$ 0.3 **2.7**	$B \to \tau\bar{e}$ 0.3 **1.6**	$B \to \tau\bar{e}$ 0.3 **1.6**	$*$
3 2	$*$	$*$	$B \to \tau\bar{e}X$ 14 $\boxed{\mathbf{11}}$	$B \to \tau\bar{e}X$ 7.2 $\boxed{\mathbf{5.5}}$	$B \to \tau\bar{e}X$ 7.2 $\boxed{\mathbf{4.1}}$	$B \to \tau\bar{e}X$ 7.2 $\boxed{\mathbf{4.1}}$	$*$
3 3	$*$	$*$	$\tau \to 3e$ 17 $\boxed{\mathbf{15}}$	$\tau \to 3e$ 14 $\boxed{\mathbf{7.6}}$	$\tau \to 3e$ 9 $\boxed{\mathbf{7.7}}$	$\tau \to 3e$ 4 **7.7**	$*$

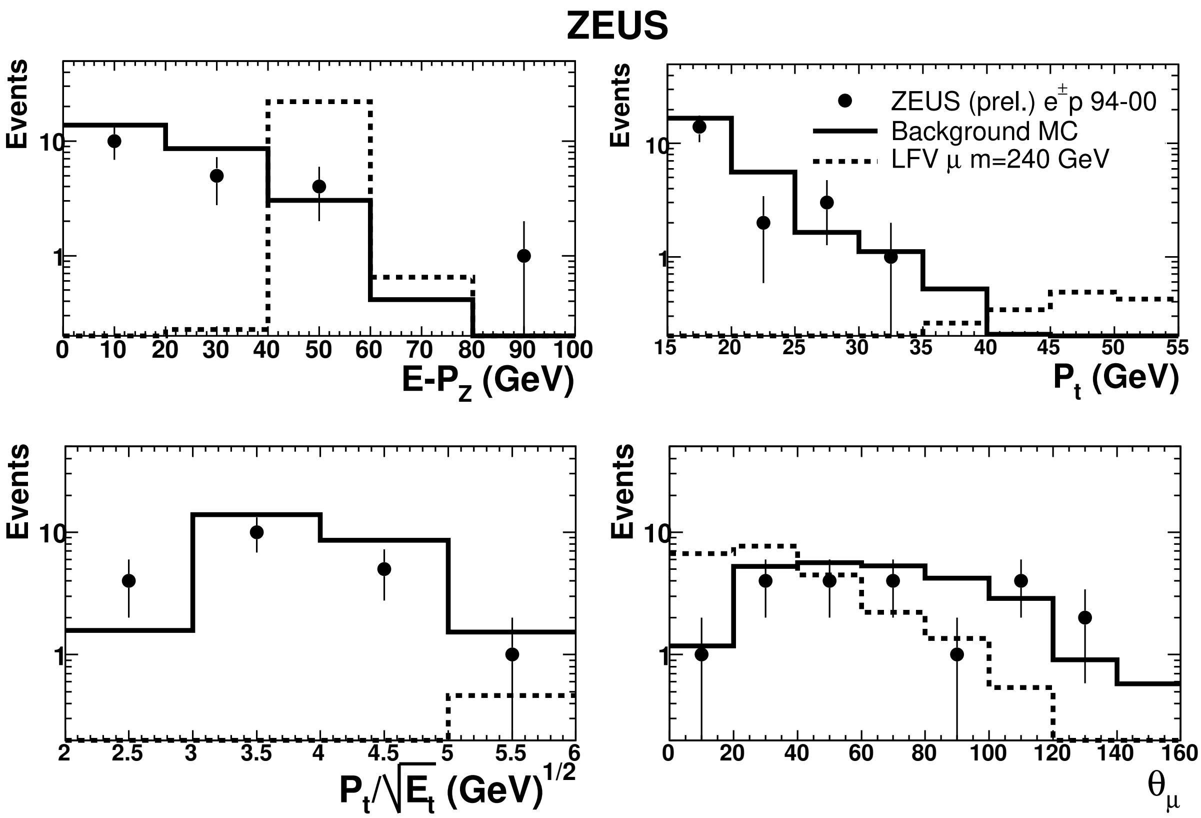

Figure 1: *Comparison between data (dots) and SM Montecarlo (solid line) for different variables ($E - P_Z$, $\not{P}_t$, $\not{P}_t/\sqrt{E_t}$, polar angle of the muon) after the μ-channel preselection. The dashed line represents the signal with arbitrary normalization.*

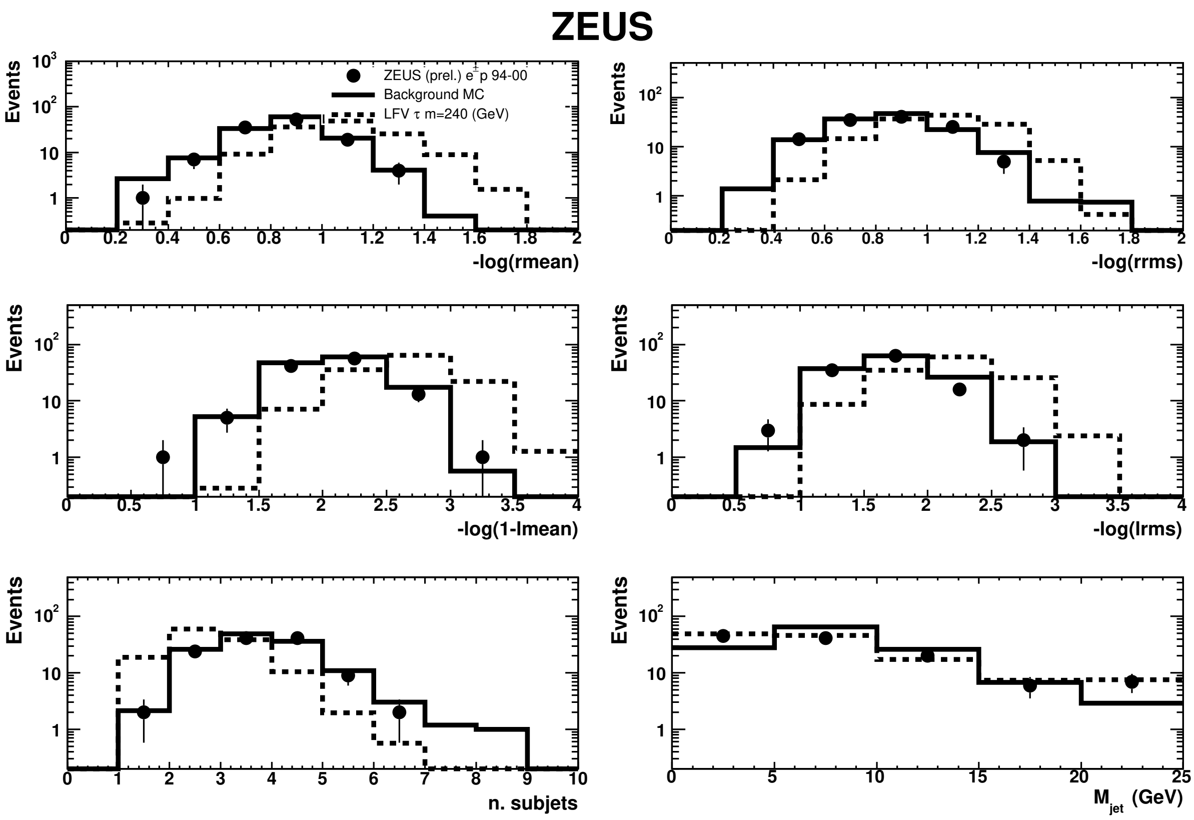

Figure 2: *Comparison between data (dots) and SM Montecarlo (solid line) for the variables used in the τ discriminant (rmean, rrms, lmean, lrms, number of subjects, jet mass) after the τ-channel preselection (hadronic τ decays). The dashed line represents the signal with arbitrary normalization.*

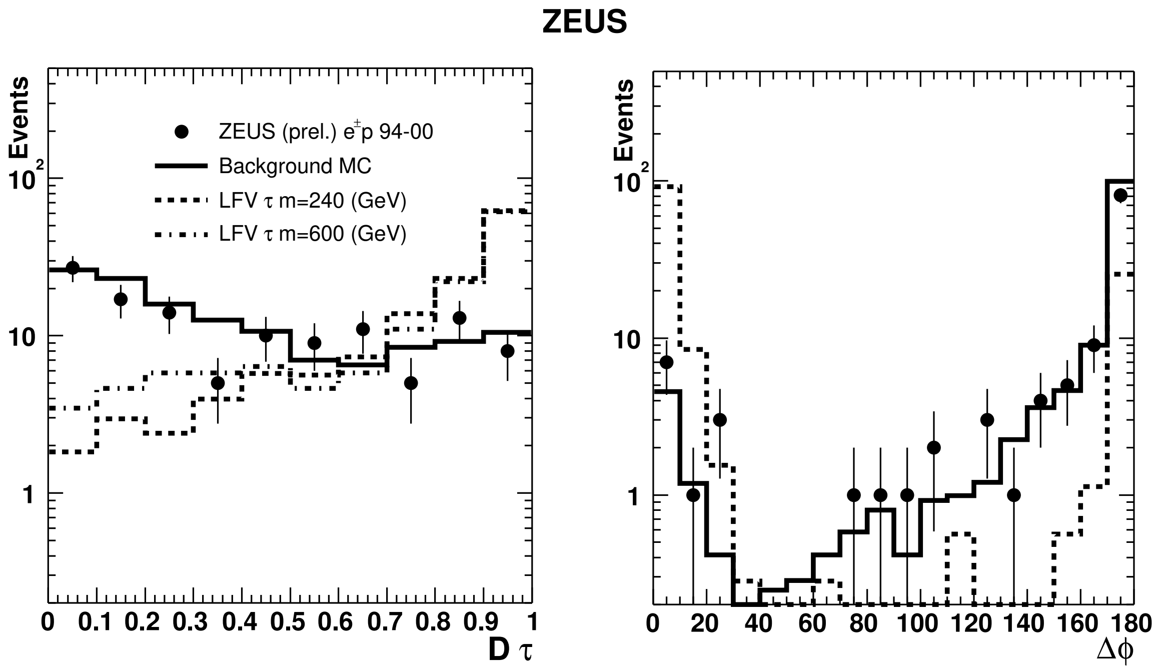

Figure 3: *Distribution of the discriminant and of $\Delta\phi$ after hadronic τ decay preselection. Dots represent 99-00 data while the solid line is the SM prediction from Montecarlo. The signal distribution for two different LQ masses* $240\,GeV$ *(dashed line) and* $600\,GeV$ *(dash-dotted line) are also shown with arbitrary normalization.*

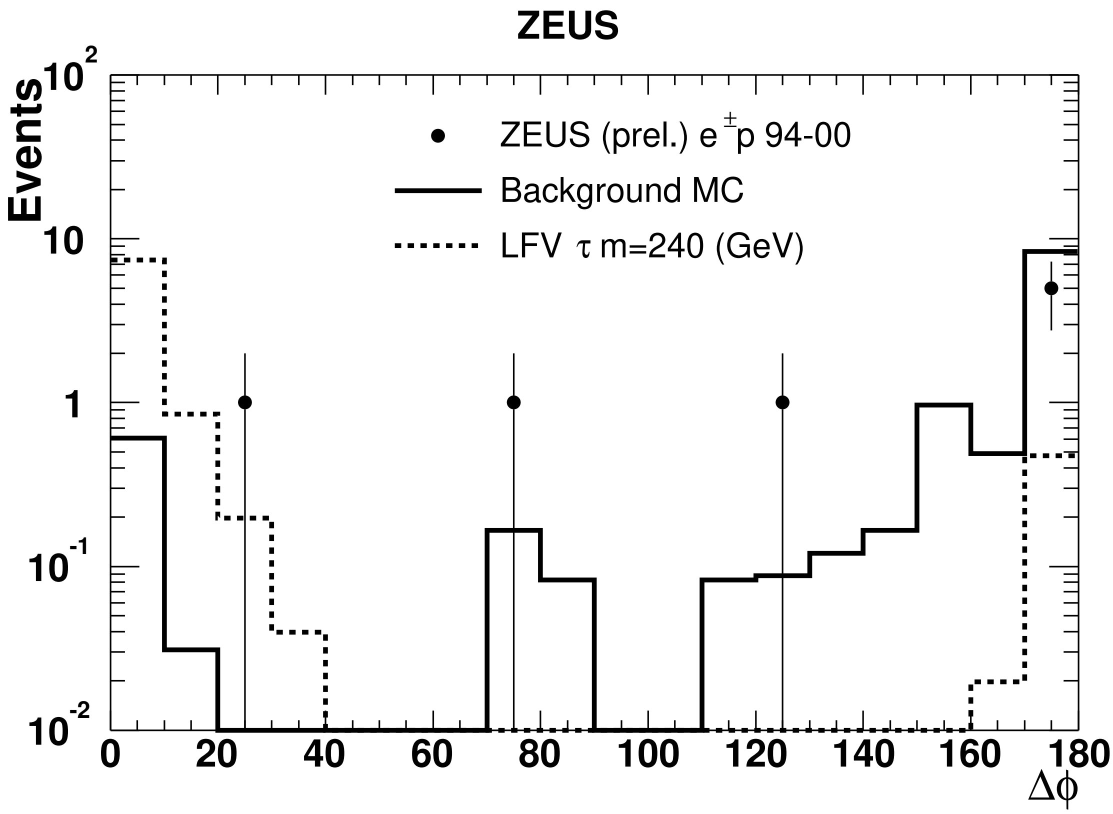

Figure 4: *$\Delta\phi$ distribution of the events with* $\mathrm{D} > 0.9$ *after hadronic τ decay preselection. Dots represent 99-00 data while the solid line is the SM prediction from Montecarlo. The dashed line represents the signal with arbitrary normalization.*

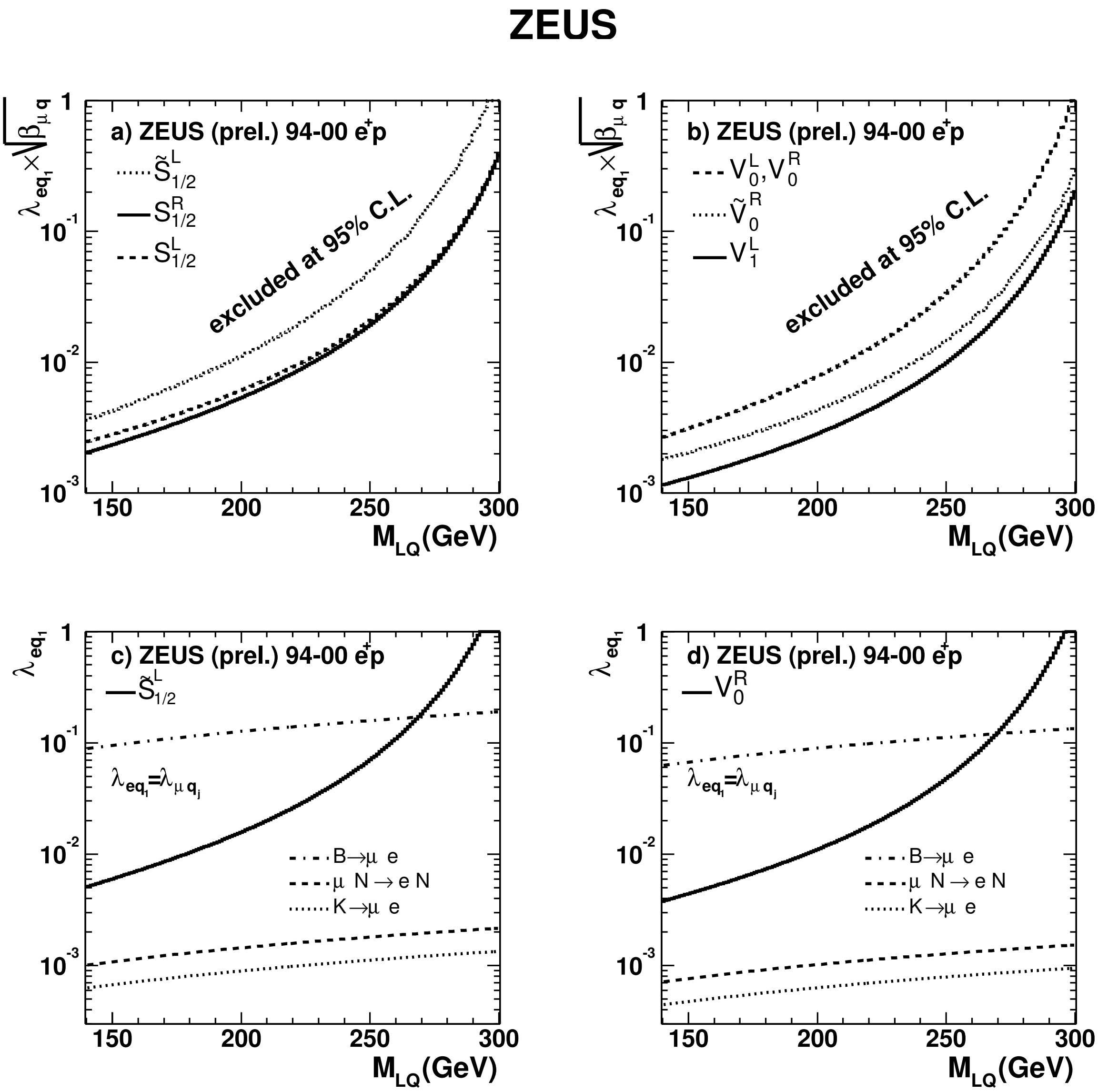

Figure 5: *Limits for $F = 0$ low mass LQs in the μ-channel obtained from e^+p collisions. The upper plots show 95% C.L. limits on $\lambda_{eq_1} \times \sqrt{\beta_{\mu q}}$ for scalar (left) and vector (right). In the lower plots ZEUS limits on λ_{eq_1} are compared to the indirect constraints from low energy experiment assuming $\lambda_{eq_1} = \lambda_{\mu q}$.*

ZEUS

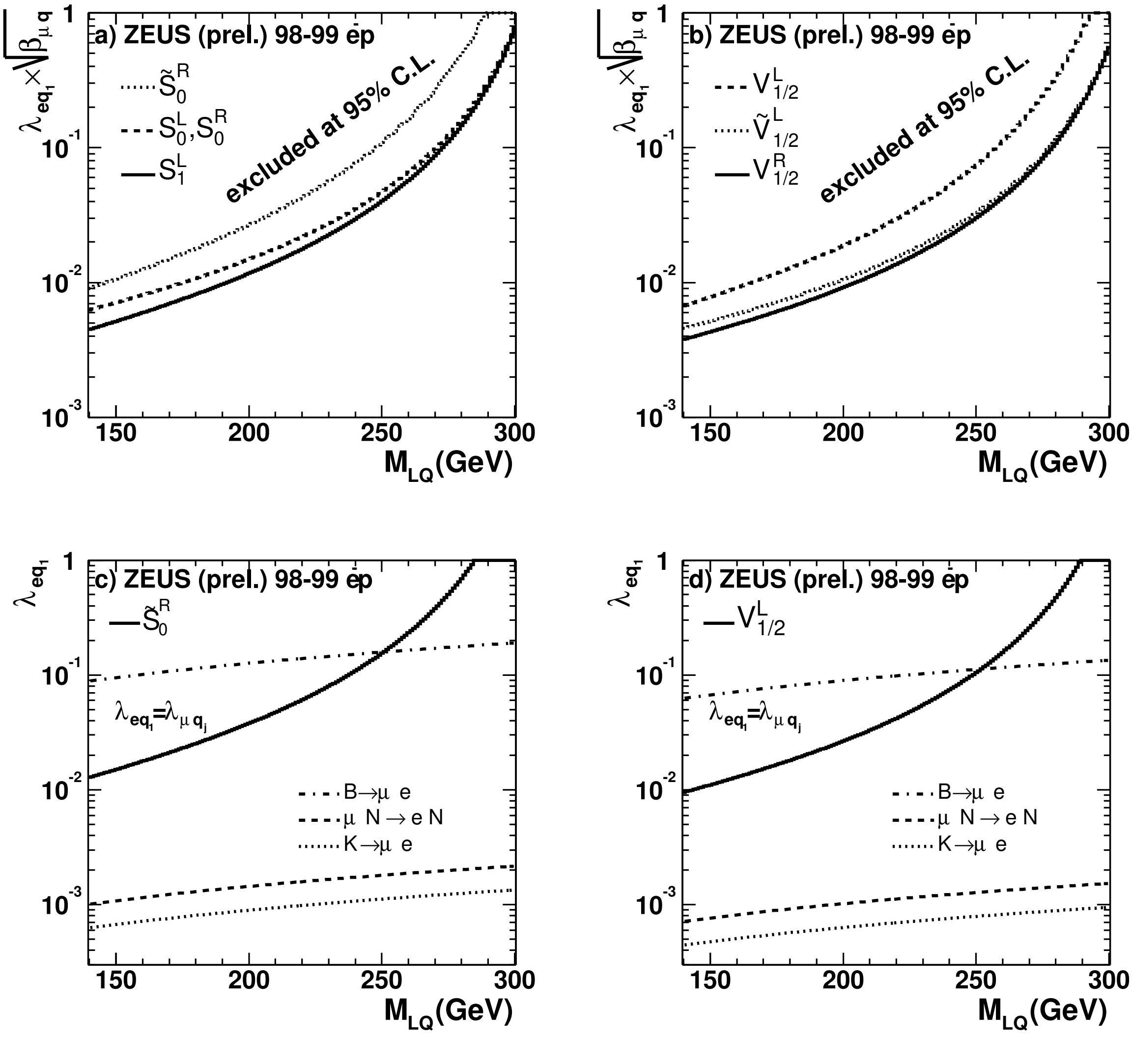

Figure 6: *Limits for $F = 2$ low mass LQs in the μ-channel obtained from e^+p collisions. The upper plots show 95% C.L. limits on $\lambda_{eq_1} \times \sqrt{\beta_{\mu q}}$ for scalar (left) and vector (right). In the lower plots ZEUS limits on λ_{eq_1} are compared to the indirect constraints from low energy experiment assuming $\lambda_{eq_1} = \lambda_{\mu q}$.*

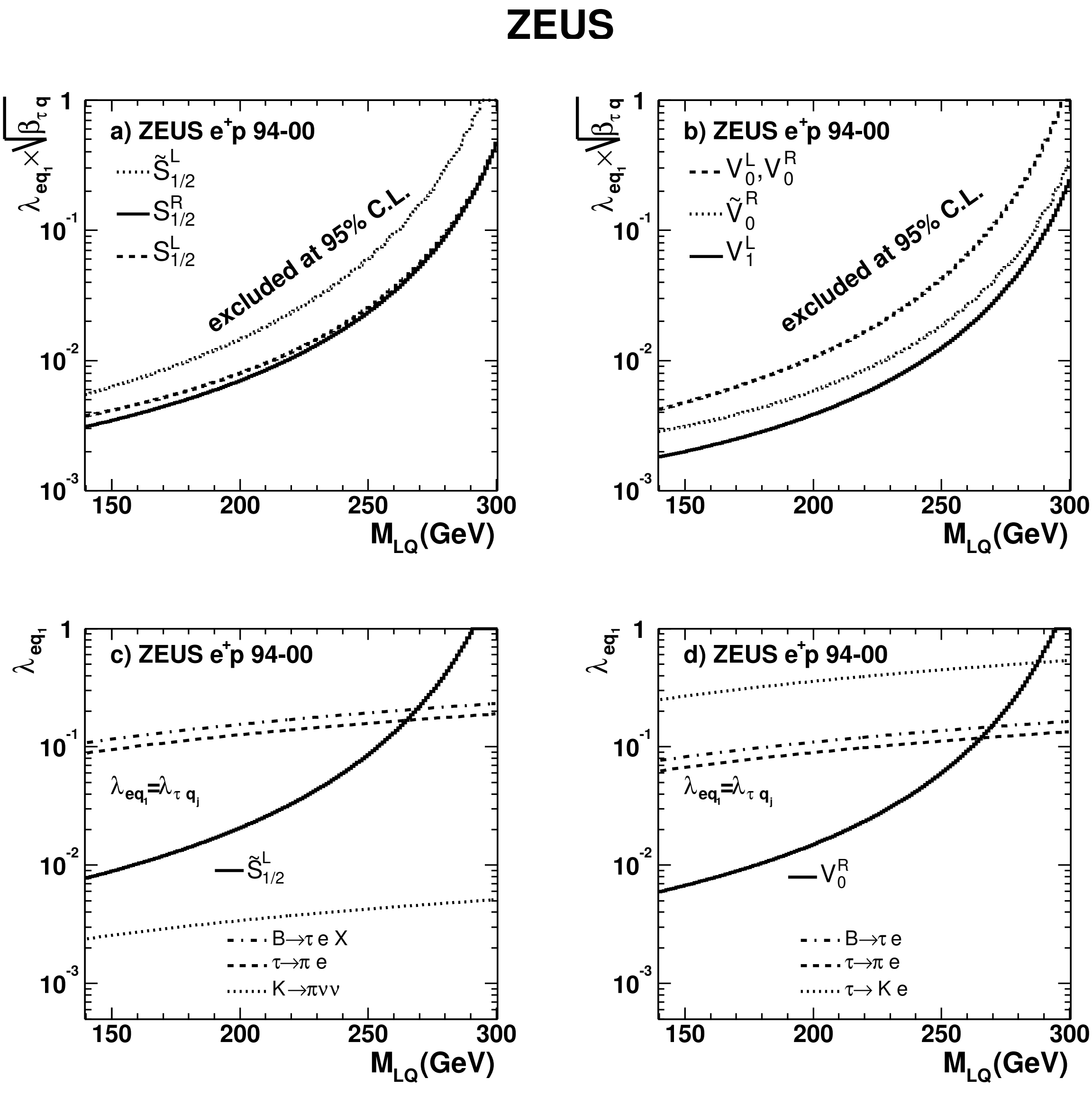

Figure 7: *Limits for $F = 0$ low mass LQs in the τ-channel obtained from e^+p collisions. The upper plots show 95% C.L. limits on $\lambda_{eq_1} \times \sqrt{\beta_{\tau q}}$ for scalar (left) and vector (right). In the lower plots ZEUS limits on λ_{eq_1} are compared to the indirect constraints from low energy experiment assuming $\lambda_{eq_1} = \lambda_{\tau q}$.*

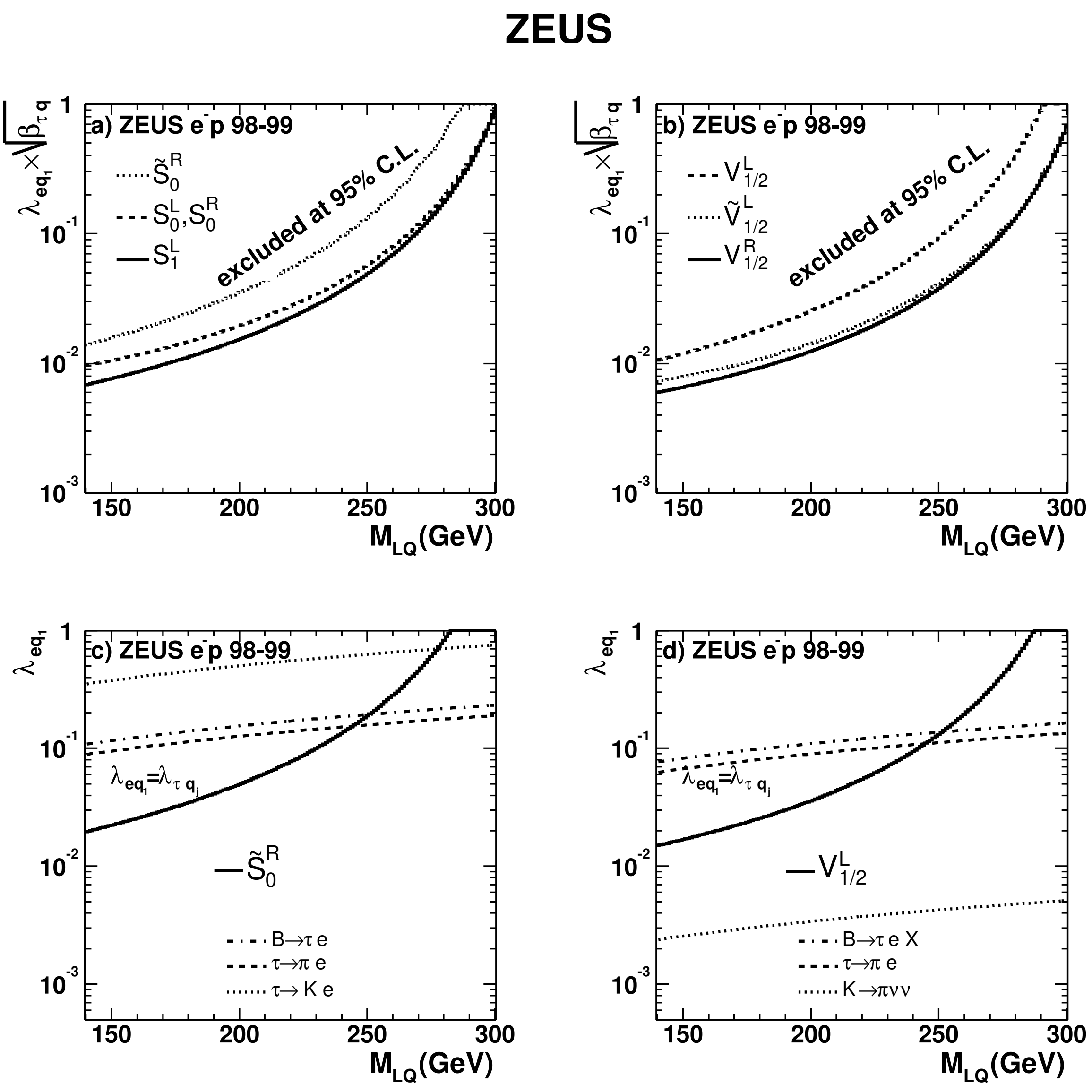

Figure 8: *Limits for $F = 2$ low mass LQs in the τ-channel obtained from e^+p collisions. The upper plots show 95% C.L. limits on $\lambda_{eq_1} \times \sqrt{\beta_{\tau q}}$ for scalar (left) and vector (right). In the lower plots ZEUS limits on λ_{eq_1} are compared to the indirect constraints from low energy experiment assuming $\lambda_{eq_1} = \lambda_{\tau q}$.*